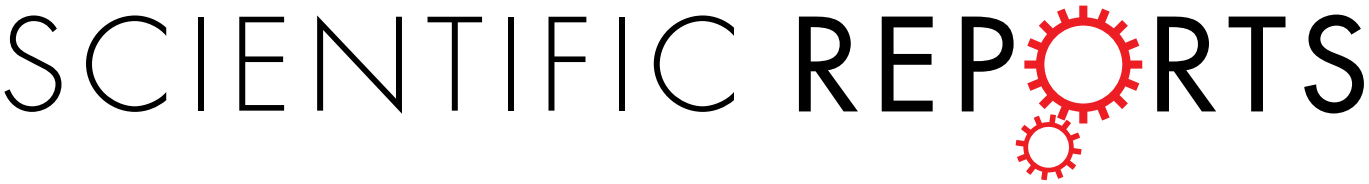

OPEN

Unconventional *exo* selectivity in thermal normal-electron-demand Diels–Alder reactions

Received: 02 June 2016
Accepted: 22 September 2016
Published: 12 October 2016

Guo-Ming Ho[1,*], Ci-Jhang Huang[2,*], Elise Yu-Tzu Li[2], Sheng-Kai Hsu[1], Ti Wu[1], Medel Manuel L. Zulueta[1], Kevin Binchia Wu[1] & Shang-Cheng Hung[1]

The Diels–Alder reaction is a useful tool for generating functionalized chiral molecules through the concerted cycloaddition of dienes and dienophiles leading to six-membered rings. Traditionally, the selective predictions of the products rely heavily on consideration of the secondary orbital interactions that stabilize the *endo* pathway. However, there remain some basic examples defying this notion and produce the *exo*-isomer as major product. Here we systematically evaluated of the structural features driving *exo* selectivity in thermal normal-electron-demand Diels–Alder reactions. Substitution at the Cβ position and the size and electronegativity of the electron-withdrawing group of the dienophile are contributing factors. Experimental and computational studies both point toward the steric and electrostatic forces between the substituents in both the diene and the dienophile that increase the likelihood of the *exo* pathway. For these substrates, the dominance of the *endo* pathway is reduced by transition state distortions and poor structural alignments of the reacting partners. We also noted the tilt of the dienophile with respect to the diene causing steric strain on the functionalities at the more advanced bond forming carbon-carbon position of the *endo* transition state. Insights into such factors may benefit synthetic planning and asserting control over this important named reaction.

Since Otto Diels and Kurt Alder announced their discovery of the pericyclic reaction involving dienes and dienophiles in 1928[1], the Diels–Alder reaction has been intensively developed and refined to become one of the most powerful carbon–carbon bond forming methods in organic chemistry[2]. This reaction enables the simultaneous regioselective formation of two σ bonds leading to six-membered rings, thereby establishing up to four stereogenic centers in a single step. Such elegant potential to control the regio- and stereochemical outcomes of inter- and intramolecular [4 + 2] cycloadditions subsequently proved a valuable resource for constructing many complex biologically active molecules and natural products[3–6].

Normal-electron-demand Diels–Alder cycloaddition can be achieved by the interaction of the highest occupied molecular orbital of an electron-rich diene (e.g., **1**) and the lowest unoccupied molecular orbital of an electron-deficient dienophile (e.g., **2**) generating the *exo* and *endo* transition states (e.g., **3** and **4**, respectively) (Fig. 1). Since Woodward and Hoffmann's proposal for secondary orbital interactions[7], *endo* selectivity has been regarded as rather predictable and considered a familiar attribute of these reactions. Thus, while *exo* addition seemed preferable over the more sterically hindered *endo* approach, secondary orbital interactions in the *endo* transition state **4** is understood to promote the formation of the *endo* cycloadduct **6** as the major product[8]. Correspondingly, *exo*-selective Diels–Alder cycloadditions occur less frequently, be it under plain thermal[9–15] or catalyzed[13,16–31] conditions. In many of these cases, suitably positioned structural features from the added catalyst or from the substrates themselves apparently override the factors that stabilize the *endo* transition state.

While preparing several versatile cyclohexanones using thermal Diels–Alder reaction, we noted some interesting cases of *exo* selectivity. Cycloaddition of the silylated dienes **7**[32] and **8**[33] with cinnamonitrile (**9**) at 140 °C for 12 h surprisingly both gave the *exo*-adducts **exo-10** and **exo-11** as major coupling products, respectively (Fig. 2a). The structures of these *exo*-adducts were confirmed by X-ray crystallographic analysis (Fig. 2b,c). The stereochemical relationships of the contiguous carbons on the cyclohexene ring of the adducts were also characterized by NMR coupling constant analysis and nuclear Overhauser effect correlation experiments (see Supplementary Methods).

[1]Genomics Research Center, Academia Sinica, 128, Section 2, Academia Road, Taipei 115, Taiwan. [2]Department of Chemistry, National Taiwan Normal University, 88, Section 4, Ting-Chow Road, Taipei 116, Taiwan. *These authors contributed equally to this work. Correspondence and requests for materials should be addressed to E.Y.-T.L. (email: eliseytli@ntnu.edu.tw) or S.-C.H. (email: schung@gate.sinica.edu.tw)

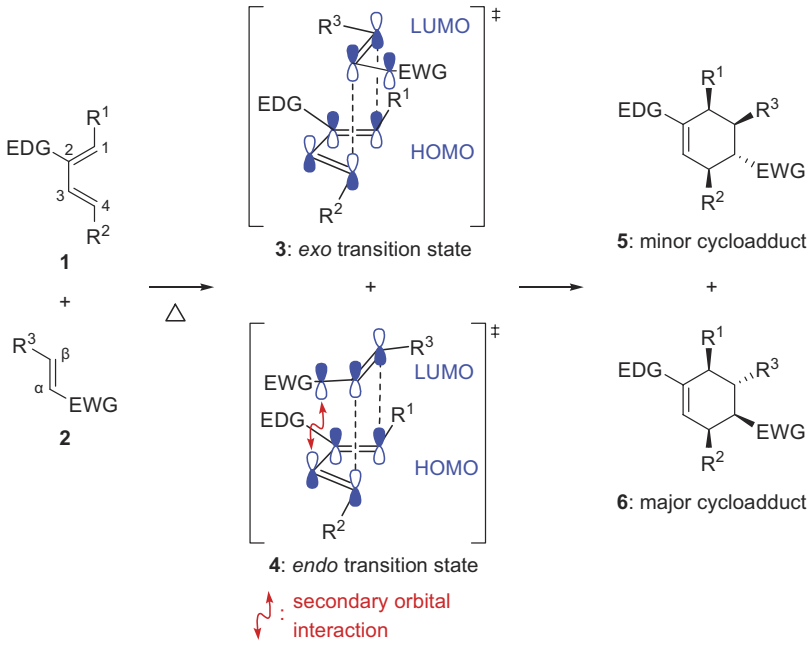

Figure 1. General stereoselective prediction for normal-electron-demand Diels–Alder reactions. EWG = electron-withdrawing group, EDG = electron-donating group, HOMO = highest occupied molecular orbital, LUMO = lowest unoccupied molecular orbital.

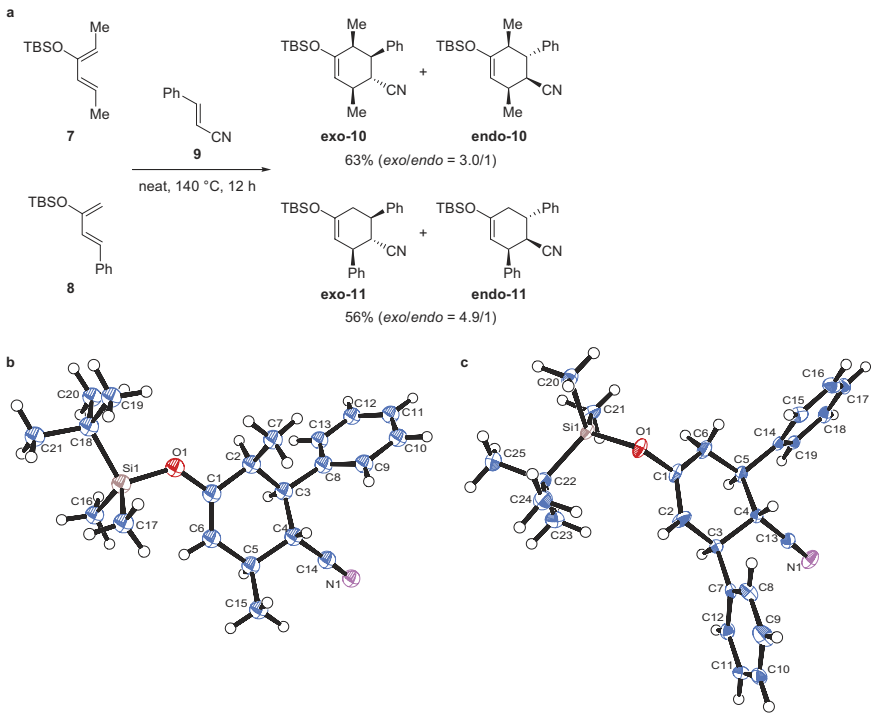

Figure 2. Diels–Alder reactions of dienes 7 and 8 with cinnamonitrile (9). (**a**) The reaction conditions and outcomes. (**b**) X-ray crystal structure of **exo-10**. (**c**) X-ray crystal structure of **exo-11**. TBS = *tert*-butyldimethylsilyl.

Isomerization of the kinetic *endo*-adduct toward the thermodynamically more stable *exo*-adduct, however, remained a possibility[34]. If such *endo*-to-*exo* isomerization occurred, the *endo*-product should accumulate at the early stage of the reaction before eventually decreasing in proportion to the *exo* isomer. However, we noted by NMR monitoring that the apparent ratios of the *exo*- and *endo*-adducts remained almost constant throughout the

process (measured at 0.5, 1, 2, 4, 8, and 12 h) (Supplementary Fig. 1). Exposure of the *endo*-adduct to the same reaction conditions for 4 h also did not produce the *exo* counterpart (Supplementary Fig. 2). In light of these results, we concluded that no *endo*-to-*exo* transformation occurred in our reactions.

Houk and co-workers also found that some Diels–Alder reactions of α,β-unsaturated *N*-acyloxazolidinones under Lewis acid-catalyzed conditions were *exo*-selective[25]. They suggested that methyl substitution at both C1 of the silylated diene and Cβ of the dienophile (for the carbon designations used in this paper, refer to Fig. 1) are necessary features that support *exo* selectivity. The lack of substituents at either of those carbons, which hold the shorter of the two σ bonds being formed in the transition states in such concerted asynchronous reactions, largely resulted in *endo* preference. As they described in these cases, the catalyst orientation likely exerted steric influence at the transition state and was partly responsible for the ultimate isomer preference.

The apparent similarity and deviation (i.e., *exo* preference for the cycloaddition of **8** and **9**) of our initial results from Houk's work stimulated us to study the structural factors that influence *exo* and *endo* stereoselectivity in thermal noncatalyzed Diels–Alder reactions involving dienes **7** and **8**. To flesh out the fundamental source of the stereoselectivity, we used simple dienophiles with different electron-withdrawing functionalities such as nitrile, aldehyde, ketone, ester and nitro groups. Lewis acid catalysts were not employed to avoid any intervening chelation or steric effects that did not originate from the diene and the dienophile themselves. We also became interested in the effects of the substitution pattern of the reactants on stereoselectivity and focused on these structural features instead of optimizing yields or determining the best conditions necessary for cycloaddition. The results of the synthetic evaluations are described herein as well as the computational studies that further shed light on the intricate details of the cycloaddition process.

Results and Discussion

Synthesis experiments. The Diels–Alder reactions of dienes **7** and **8** were carried out with a series of acyclic dienophiles bearing electron-withdrawing groups and with different substitution patterns at the Cα and Cβ positions (Table 1). We opted for variations that involved either methyl or phenyl group at the Cβ position in *trans* orientation with respect to the electron-withdrawing group or a methyl group at the Cα position to examine the influence of the reactant substituents on the *exo* and *endo* selectivity. The thermal [4 + 2] cycloadditions were performed in a sealed tube at 120–180 °C under neat conditions or in the presence of xylene (at 140 °C) or toluene (at 120 °C, in some nitroolefin cases) as solvent (see the Supplementary Methods for the detailed conditions). The *tert*-butyldimethylsilyl moiety remained intact throughout the process allowing the enol ether state to be preserved and characterized, albeit with double bond migration in some cases as mentioned below. The *exo* and *endo* assignments of the cycloadducts were based on the results of extensive NMR experiments (see Supplementary Methods) and X-ray crystallographic analysis in the cases of **exo-31**, **endo-62**, **exo-64** and **exo-67** (Supplementary Fig. 3). We similarly checked the possibility of *endo*-to-*exo* isomerization, this time with **endo-52** as representative compound, but no such transformation was again observed (Supplementary Fig. 2). Aside from the usual adducts, cycloaddition with diene **7** also gave, in some instances, products resulting from the migration of the double bond toward the adjacent, more substituted position. A similar phenomenon was also observed by Nakashima and Yamamoto in Brønsted acid-catalyzed Diels–Alder addition of 1,4-dimethyl silyloxydiene with ethyl vinyl ketone[35]. Because we are interested in observing the ultimate *exo* and *endo* selectivities, the quantities of these migration products were combined with the values of their parent *exo* or *endo* adducts.

The presence of functionalities at the C1 and C4 positions of the diene and the variations in the dienophiles provided some interesting general trends. For cycloadditions with diene **7**, excellent *exo* selectivities were observed with Cβ-methylated dienophiles (i.e., compounds **18**, **27**, **39**, **51** and **63**) in all the compound classes tested. Replacement of the Cβ-methyl with phenyl group still furnished the *exo*-cycloadducts as major products albeit in moderate-to-good stereoselectivity. The attributes brought about by these functional groups, thus, were able to considerably prevail over the factors, mainly secondary orbital interaction, often invoked to favour the *endo* pathway[8]. Absence of a substituent at Cβ resulted in either stereorandomness or a plunge into the "normal" *endo* territory. The same observation remained true even when a methyl group is positioned at Cα. Comparing the cycloaddition outcomes involving the related Cβ-unsubstituted carbonyl-containing dienophiles, the α,β-unsaturated aldehydes displayed the best tendency to form the *endo*-adduct, followed by the corresponding methyl ketones, and with the methyl ester losing much of the *endo* selectivity. A methyl group at the Cα position appeared to further increase the *endo* selectivity in the aldehyde (with dienophile **24**) and ketone (with dienophile **36**) cases. The stereorandom outcomes seen for the Cβ-unsubstituted nitrile and ester classes as opposed to that of aldehydes and ketones are suggestive of the roles of the electron-rich oxygen (from the methoxy group) and nitrogen atoms in the transition state preference of the reactants. For cycloadditions with nitroolefins, an early study by Node and co-workers[10] noted that *exo* selectivity was a feature of Diels–Alder cycloadditions of 1-methoxy-3-trimethylsilyloxy-1,3-butadiene (Danishefsky's diene) with Cβ-substituted nitroolefins. This *exo* preference was linked to the destabilization of the *endo* transition state as a result of the electrostatic repulsion between the silyloxy group of the diene and the nitro group of the dienophile. In our case, cycloadditions with nitroolefins behaved similarly as with other dienophile classes, and moderate inclination toward *endo* was observed when Cβ is unsubstituted.

Substitution, particularly with a methyl group, at C1 of the diene was found necessary for *exo* selectivity in Lewis acid-catalyzed cycloadditions with Cβ-methylated dienophiles[25]. However, despite the lack of substitution at the C1 position of diene **8**, our experiments showed that the *exo*-isomers remained the dominant products in Diels–Alder cycloadditions with Cβ-substituted olefins. It was noted in such cases that, compared to cycloadditions with diene **7**, the magnitude of the differences in the *exo* preference between dienophiles with methyl and phenyl substitution at the Cβ position became less evident. To illustrate, note the differences in the ratio of the ester *exo*/*endo*-adducts between **52** (>20/1) and **55** (2.6/1) both of which were derived from **7** as opposed to **53** (2.7/1) and **56** (1.6/1) both of which were derived from **8**. The absence of an interfering functionality at C1 of

Dienophile	Cycloaddition with 7			Cycloaddition with 8		
	Product	Yield[a]	*exo*/*endo*[b]	Product	Yield[a]	*exo*/*endo*[b]
12: $R^1 = R^2 = H$, EWG = CN	**13**	60%	1/1	**14**	54%	3.3/1
15: $R^1 = H$, $R^2 = Me$, EWG = CN	**16**	65%	1.2/1	**17**	55%	1.3/1
18: $R^1 = Me$, $R^2 = H$, EWG = CN	**19**	57%	>20/1	**20**	55%	4.0/1
21: $R^1 = R^2 = H$, EWG = C(O)H	**22**	74%	1/2.1	**23**	63%	1/1
24: $R^1 = H$, $R^2 = Me$, EWG = C(O)H	**25**	96%	1/4.6	**26**	73%	1/2.7
27: $R^1 = Me$, $R^2 = H$, EWG = C(O)H	**28**	79%	>20/1[c]	**29**	42%	1.8/1
30: $R^1 = Ph$, $R^2 = H$, EWG = C(O)H	**31**	70%	3.0/1	**32**	45%	1.9/1
33: $R^1 = R^2 = H$, EWG = C(O)Me	**34**	64%	1/1.3[d]	**35**	99%	1/1.1
36: $R^1 = H$, $R^2 = Me$, EWG = C(O)Me	**37**	83%	1/2.8[e]	**38**	93%	1/1
39: $R^1 = Me$, $R^2 = H$, EWG = C(O)Me	**40**	89%	19/1[f]	**41**	71%	2.3/1
42: $R^1 = Ph$, $R^2 = H$, EWG = C(O)Me	**43**	92%	5.3/1	**44**	65%	1.9/1
45: $R^1 = R^2 = H$, EWG = CO_2Me	**46**	73%	1.1/1	**47**	29%	1.3/1
48: $R^1 = H$, $R^2 = Me$, EWG = CO_2Me	**49**	79%	1.3/1	**50**	44%	1.2/1
51: $R^1 = Me$, $R^2 = H$, EWG = CO_2Me	**52**	79%	>20/1[g]	**53**	32%	2.7/1
54: $R^1 = Ph$, $R^2 = H$, EWG = CO_2Me	**55**	89%	2.6/1[h]	**56**	63%	1.6/1
57: $R^1 = R^2 = H$, EWG = NO_2	**58**	66%	1/2.8	**59**	62%	2.3/1
60: $R^1 = H$, $R^2 = Me$, EWG = NO_2	**61**	67%	1/1.9	**62**	75%	1.8/1
63: $R^1 = Me$, $R^2 = H$, EWG = NO_2	**64**	64%	19/1	**65**	60%	4.3/1
66: $R^1 = Ph$, $R^2 = H$, EWG = NO_2	**67**	76%	3.8/1	**68**	80%	5.7/1

Table 1. Thermal Diels–Alder reactions of dienes 7 and 8 with various dienophiles.

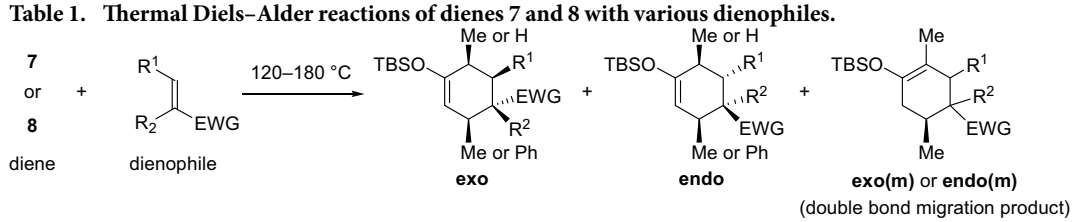

[a]Based on the total isolated amounts of the isomers. [b]Determined from the ^1H NMR spectra of the crude product mixture with the amount for the double bond migration isomer included in the corresponding *exo* or *endo* values. [c]**exo(m)-28** is 17% of *exo* selectivity. [d]**endo(m)-34** is 68% of *endo* selectivity. [e]**endo(m)-37** is 4% of *endo* selectivity. [f]**exo(m)-40** is 4% of *exo* selectivity. [g]**exo(m)-52** is 33% of *exo* selectivity. [h]**endo(m)-55** is 21% of *endo* selectivity.

diene **8**, which may provide more steric repulsion to the three-dimensional methyl than to the flat phenyl group at Cβ, was the probable reason for the reduced selectivity difference. Interestingly, diene **8** provided a modest increase in *exo* preference in the cycloaddition with the Cβ-unsubstituted dienophiles as compared to diene **7**. This result is likely due to the subtle steric influence of the wider C4-phenyl group on the electron-withdrawing group in the *endo* pathway. In these cases, only methacrolein (**24**) supplied meaningful *endo* selectivity. Moreover, the best *exo*-selective outcomes were noted from dienophiles holding nitrile and nitro groups—the most electron-egative electron-withdrawing groups in this series.

Further replacement of the C4-phenyl in **8** with methyl group and cycloaddition with the same set of α,β-unsaturated ketones (Supplementary Table 1) provided a blend of selectivities characteristic of both dienes **7** and **8** (i.e., less pronounced difference in *exo* selectivity between the Cβ-substituted dienophiles **39** and **42** and substantial *endo* selectivity with Cα-methylated dienophile **36**). These comparisons suggest steric strain between the C4-methyl group of the diene and the Cα-methyl group of the dienophile, destabilizing the *exo* transition state—a destabilization that was not as extensive as when a phenyl group was present at C4.

Transition State Computations. Density functional theory calculations were performed to examine the *exo* and *endo* reaction pathways using B3LYP[36,37] and M06-2X[38] hybrid functionals with 6-311++G(d,p)[39,40] basis sets. The electronic activation barriers ($\Delta E_a^{\ddagger}$) and the free energies of activation ($\Delta G_a^{\ddagger}$) for the *endo* and *exo* pathways involving diene **7** are presented in Supplementary Table 2 and Supplementary Table 3, respectively, and those for diene **8** are presented in Table 2 and Supplementary Table 4, respectively. The correlations between the experimental observations and the respective theoretically calculated $\Delta E_a^{\ddagger}$ and $\Delta G_a^{\ddagger}$ are shown in Supplementary Fig. 4 and Supplementary Fig. 5. Our M06-2X calculations generally produced lower activation energies than B3LYP, but in many of the studied cases, the B3LYP and M06-2X functionals were consistent and gave similar trends. For both functionals, about 70% to 80% of the calculated trends (*exo* vs *endo* selectivity) agreed qualitatively with the experiments and fall within the shaded region in Supplementary Fig. 4 and Supplementary Fig. 5. In particular, both functionals reproduced, with only a few exceptions, the experimental observations that cycloaddition reactions yield high *exo* selectivity if the Cβ position is substituted, especially with a methyl group (i.e., using dienophiles **18**, **27**, **39** and **51**). Notable outliers were the calculation results for nitroolefins, which often failed to mimic

Dienophile: substituent	$\Delta E_a^{\ddagger}$ (kcal/mol)		k_{exo}/k_{endo} [b]
	Exo	*Endo*	
12: EWG = CN	16.9 (13.4)	17.8 (12.9)	2.8/1 (1/1.9)
15: α-Me, EWG = CN	20.3 (14.2)	20.8 (13.7)	1.8/1 (1/1.9)
18: β-Me, EWG = CN	21.8 (15.5)	23.0 (16.2)	4.2/1 (2.3/1)
11: β-Ph, EWG = CN	23.9 (12.0)	24.5 (14.9)	1.9/1 (33/1)
21: EWG = C(O)H	16.9 (13.8)	16.9 (12.6)	1/1 (1/4.5)
24: α-Me, EWG = C(O)H	19.4 (13.8)	18.5 (12.7)	1/3.3 (1/4.2)
27: β-Me, EWG = C(O)H	20.8 (15.3)	21.2 (15.4)	1.6/1 (1.2/1)
30: β-Ph, EWG = C(O)H)	24.7 (14.1)	24.6 (16.2)	1/1.2 (13/1)
33: EWG = C(O)Me	19.1 (14.5)	19.1 (12.8)	1/1 (1/7.6)
36: α-Me, EWG = C(O)Me	21.4 (13.7)	20.4 (12.8)	1/3.5 (1/3.3)
39: β-Me, EWG = C(O)Me	24.1 (16.5)	24.3 (16.2)	1.4/1 (1/1.4)
42: β-Ph, EWG = C(O)Me	26.5 (14.4)	26.2 (15.7)	1/1.3 (5.0/1)
45: EWG = CO_2Me	18.7 (14.0)	19.2 (12.6)	2.0/1 (1/5.2)
48: α-Me, EWG = CO_2Me	20.7 (13.7)	20.9 (13.4)	1.4/1 (1/1.5)
51: β-Me, EWG = CO_2Me	21.4 (13.8)	22.8 (15.0)	5.6/1 (4.2/1)
54: β-Ph, EWG = CO_2Me	25.2 (12.6)	26.0 (15.6)	2.9/1 (36/1)
57: EWG = NO_2	10.6 (6.6)	9.9 (5.0)	1/2.5 (1/7.4)
60: α-Me, EWG = NO_2	12.8 (7.5)	12.1 (5.4)	1/2.3 (1/13)
63: β-Me, EWG = NO_2	14.8 (6.8)	14.7 (8.7)	1/1.5 (1/10)
66: β-Ph, EWG = NO_2	16.7 (6.0)	16.0 (6.0)	1/2.2 (1/1)

Table 2. Calculated activation energy barriers ($\Delta E_a^{\ddagger}$) and product ratios of the Diels–Alder reaction pathways involving diene 8 by B3LYP and M06-2X functionals[a]. [a]The results of the M06-2X calculations are given in parenthesis. [b]Relative reaction rate constants estimated by the Arrhenius equation[52].

the selectivity trend in the experiments. On the other hand, calculations corresponding to dienophiles with no substituent at the Cβ positions produced the *endo*-isomer as major products, except in the nitrile and ester cases wherein the *exo* pathways were largely favoured. Overall, our computations suggest, as with the experimental observations, that better *exo* selectivity can be achieved with α,β-unsaturated nitriles and esters and less so with the corresponding aldehydes and ketones.

Previous studies[41–43] suggested that the M06-2X functional gives better free energy values for concerted cycloadditions due to sensible treatment of medium-range correlation effects, such as van der Waals interactions[38]. For some Cβ-phenyl substituted dienophiles (e.g., **30** and **42**), the B3LYP functional predicted *endo* selectivities upon cycloaddition with diene **8**, but M06-2X calculations showed *exo* selectivities, matching those observed experimentally for such cases (Table 2). Nevertheless, we also noted that, compared with experimental observations, the M06-2X functional overstabilized the *exo* with respect to the *endo* pathway when the Cβ position is substituted with a phenyl group. With lower mean absolute error for both $\Delta E_a^{\ddagger}$ and $\Delta G_a^{\ddagger}$, the B3LYP results appeared to correlate better with experiments over M06-2X for this set of reactions (Supplementary Fig. 4 and Supplementary Fig. 5).

To rationalize the origin of the unusually high *exo* selectivity found in the C1-unsubstituted diene **8** and to further examine the difference between the activation energies of the *endo* and *exo* pathways, we decomposed the $\Delta E_a^{\ddagger}$ listed in Table 2 (and also Supplementary Table 2) into their component distortion energies ($\Delta E_d^{\ddagger}$) and interaction energies ($\Delta E_i^{\ddagger}$) following previous literature[25,44,45]. $\Delta E_d^{\ddagger}$ is the difference between the energies of the reactants in the optimized geometries and the same molecules in the transition state conformations but without interactions in between them. $\Delta E_i^{\ddagger}$, on the other hand, is the difference between the energies of the reactants in the transition state conformations summed separately and the energy of the entire transition state complex. $\Delta E_a^{\ddagger}$ is then the sum of $\Delta E_d^{\ddagger}$ and $\Delta E_i^{\ddagger}$.

Table 3 shows the activation energy decompositions for the [4 + 2] cycloadditions of dienes **7** and **8** with carbonyl-containing dienophiles functionalized with a methyl group at the Cβ position. In general, the M06-2X optimizations led to structures in closer proximity, hence a much larger interaction between the diene and the dienophile fragments in the transition state and a lower total $\Delta E_a^{\ddagger}$ than those calculated by B3LYP. The *endo* pathways involving diene **7** have larger stabilizing $\Delta E_i^{\ddagger}$ over *exo* as predicted by both B3LYP and M06-2X functionals. Nevertheless, the generally smaller $\Delta E_d^{\ddagger}$ in the *exo* pathway (1–3 kcal/mol less than that in the *endo* pathway) dominated and determined the final product selectivity. Conversely, we observed a slightly larger stabilizing $\Delta E_i^{\ddagger}$ in the *exo* than in the *endo* pathway in the B3LYP calculations for diene **8**. The overall distortion was also diminished when compared to that of diene **7**, which may be chiefly attributed to the lack of substitution at the C1 position of **8**. Moreover, the stabilization from $\Delta E_i^{\ddagger}$ for cycloadditions with diene **8** were about 4–5 kcal/mol lower than the values with diene **7** as predicted by both functionals, regardless of pathway. The B3LYP computations suggested a largely diminished $\Delta E_i^{\ddagger}$ stabilizing the *endo* pathway when the 1,4-dimethyl-substituted **7** was replaced by the C4-phenyl-substituted **8**. For reactions involving diene **8**, decompositions with M06-2X produced a much larger interaction between the diene and the dienophile fragments in the transition state, giving rise to lower total $\Delta E_a^{\ddagger}$. The total $\Delta E_d^{\ddagger}$, however, remained roughly the same regardless of the choice of functionals.

Diene	Dienophile	Pathway	$\Delta E_d^{\ddagger}$ (kcal/mol)			$\Delta E_i^{\ddagger}$ (kcal/mol)
			Diene	Dienophile	Total	
7	aldehyde **27**	*Exo*	15.8 (17.6)	14.5 (11.7)	30.3 (29.3)	−7.9 (−15.3)
		Endo	16.3 (17.8)	16.4 (13.1)	32.7 (30.9)	−8.9 (−15.3)
	ketone **39**	*Exo*	16.6 (17.8)	15.7 (12.7)	32.3 (30.5)	−7.0 (−14.3)
		Endo	17.1 (18.3)	17.7 (13.2)	34.8 (31.5)	−7.8 (−14.9)
	ester **51**	*Exo*	16.2 (16.5)	13.8 (10.5)	30.0 (27.0)	−6.9 (−14.3)
		Endo	17.1 (19.2)	15.7 (10.7)	32.8 (29.9)	−7.2 (−14.9)
8	aldehyde **27**	*Exo*	11.8 (15.2)	13.5 (10.3)	25.3 (25.5)	−4.5 (−10.3)
		Endo	11.4 (15.7)	13.9 (10.9)	25.3 (26.6)	−4.1 (−11.2)
	ketone **39**	*Exo*	12.6 (14.9)	15.0 (11.9)	27.6 (26.8)	−3.6 (−10.4)
		Endo	12.3 (16.4)	15.6 (11.8)	27.9 (28.2)	−3.6 (−12.0)
	ester **51**	*Exo*	12.4 (15.1)	13.2 (9.5)	25.6 (24.6)	−4.3 (−10.7)
		Endo	12.5 (16.2)	13.4 (10.6)	25.9 (26.8)	−3.1 (−11.7)

Table 3. Decomposition of $\Delta E_a^{\ddagger}$ into distortion ($\Delta E_d^{\ddagger}$) and interaction energies ($\Delta E_i^{\ddagger}$) for the reactions between dienes 7 and 8 and the Cβ-methylated carbonyl-containing dienophiles calculated by B3LYP and M06-2X functionals[a]. [a]The relevant $\Delta E_a^{\ddagger}$ are listed in Table 2 and Supplementary Table 2. The results of the M06-2X calculations are given in parenthesis.

The M06-2X results for **8** predicted stronger stabilizing $\Delta E_i^{\ddagger}$ in the *endo* pathway (by around 1–1.6 kcal/mol), consistent with the traditional picture for secondary orbital interaction[46]. The overall *exo* selectivity, nevertheless, came from the smaller $\Delta E_d^{\ddagger}$ in the *exo* pathway. Hence, the two functionals predicted slightly different underlying mechanisms for the *exo* selectivity of diene **8**—interaction energy-driven versus distortion energy-driven. We imagined the observed *exo* selectivity as a possible combination of both factors, that is, the usual governing *endo* pathway lost its dominance due to stronger transition state distortion and/or weaker stabilization occurred in the *endo* transition state due to poor structural alignment.

We then analyzed the critical geometric parameters of the transition states involving diene **8** and the α,β-unsaturated nitriles and esters, the two most *exo*-selective dienophile classes calculated by B3LYP (Table 4, also see Supplementary Table 5). The corresponding parameters derived from cycloadditions with diene **7** are listed in Supplementary Table 6. Between the two incipient carbon–carbon bonds, Table 4 shows a much shorter $d_{1-\beta}$ (bond distance between C1 of diene and Cβ of dienophile, about 1.9 Å) than $d_{4-\alpha}$ (bond distance between C4 of diene and Cα of dienophile, about 2.9 Å), indicating the typical asynchronous behavior in most asymmetric Diels–Alder reactions[47]. In particular, we observed that $d_{1-\beta}$ was usually slightly longer in *endo* than in *exo* transition states, implying larger steric hindrance within the proximity of C1 and Cβ in the *endo* pathway, despite the lack of substitution at C1. Curiously, while $d_{1-\beta}$ remained essentially the same across the range of dienophiles examined, $d_{4-\alpha}$ was notably shorter for Cβ-substituted (2.75–2.86 Å) than Cβ-unsubstituted dienophiles (2.92–2.98 Å). Turning to cycloadditions with diene **7**, the $d_{4-\alpha}$ values were even shorter and more so for cycloadditions with Cβ-substituted dienophiles (2.38–2.62 Å). These observations suggested that the steric repulsion experienced by the Cβ (or C1) functionality prompted the shortening of $d_{4-\alpha}$ (a seesaw-like effect). We suspect that the short $d_{4-\alpha}$ in the pathways with diene **7** consequently translated into the high $\Delta E_i^{\ddagger}$ indicated in Table 3. Table 4 also lists the deviations of the dienophiles from planarity in the transition state geometry. The *endo* pathways showed much larger deviations from planarity than the *exo* counterparts by about 6° or more, further offering support for the larger distortion in the *endo* transition state.

In accordance with the twist asynchronous model[48], we also analyzed the twisting given by the C4-C1–Cβ-Cα dihedral angle as a means of balance between stress alleviation and interaction of the reacting partners (Table 4). The twisting angles in the *exo* pathway showed tendencies to push the electron-withdrawing group outward, away from the C4-phenyl group of diene **8**. The *endo* pathway, on the other hand, held the electron-withdrawing group under the repulsive influence of the silyloxy and C4-phenyl groups, minimizing the twisting. The repulsion of the Cα-methyl by the C4-phenyl group in the pathways involving the dienophiles **15** and **48** also strongly countered the phenyl repulsion of the nitrile and ester groups. This is evidenced, for example, by the smaller outward twist for the *exo* (−5°) than the *endo* pathway (−11°) with the Cα-methylated **15**. In contrast, the *exo* transition state involving the unmethylated dienophile **12** supplied a twist angle of −15°. The dienophile was also tilted at an angle in reference to the plane of the diene with the nearest point at the C1–Cβ junction (Fig. 3, also see Supplementary Fig. 6). This, in turn, brought the Cβ-substituent under the greater influence of the attached moieties at C1. Such pressure on the Cβ-substituent was not evident in the *exo* pathway and even though some degree of outward twisting would bring the Cβ-substituent somewhat in closer proximity to the silyloxy group, the experiments and calculations showed that the preference for the *exo* pathway was usually maintained.

Based on the acquired data, an underlying mechanism may be proposed for the unconventional *exo* selectivity in this series of Diels–Alder reactions. The stereoselectivity is derived from the interplay between different interaction forces in two pathways. Specifically, these include (i) the steric repulsion between the Cβ-substituent of the dienophile and the silyloxy group and C1-substituent (if any) of the diene in the *exo* pathway, (ii) the steric repulsion of groups at C1 and the Cβ-substituent as a consequence of dienophile tilting in the *endo* pathway and (iii) the steric repulsion between the electron-withdrawing group and Cα-substituent (if any) of the dienophile and the C4-substituent of the diene (Fig. 4). Twisting along the shorter forming bond in the transition state relieves

Dienophile: substituent	Pathway	Forming bond length (Å)[a]		Deviation from planarity[b]	Twist angle[c]
		$d_{1-\beta}$	$d_{4-\alpha}$		
12 (EWG = CN)	*Exo*	1.96	2.95	19°	−15°
	Endo	1.98	2.92	25°	−5°
15 (α-Me, EWG = CN)	*Exo*	1.96	2.95	22°	−5°
	Endo	1.98	2.93	28°	−11°
18 (β-Me, EWG = CN)	*Exo*	1.95	2.86	22°	−19°
	Endo	1.97	2.86	28°	3°
11 (β-Ph, EWG = CN)	*Exo*	1.94	2.80	23°	−20°
	Endo	1.96	2.75	31°	2°
45 (EWG = CO_2Me)	*Exo*	1.96	2.98	20°	−16°
	Endo	1.97	2.94	28°	−11°
48 (α-Me, EWG = CO_2Me)	*Exo*	1.97	2.96	22°	−5°
	Endo	1.97	2.98	29°	−16°
51 (β-Me, EWG = CO_2Me)	*Exo*	1.95	2.86	23°	−20°
	Endo	1.97	2.86	33°	−4°
54 (β-Ph, EWG = CO_2Me)	*Exo*	1.93	2.81	23°	−21°
	Endo	1.96	2.75	36°	−3°

Table 4. Critical geometrical parameters of the *exo* and *endo* transition states of Diels–Alder reactions involving diene 8 calculated at B3LYP/6-311++G(d,p) level. [a]The subscripts represent the carbons involved in bond formation. [b]Deviation from planarity of the dienophile spanning from the EWG to the *trans*-β -function. [c]Deviation of the diene and dienophile from being parallel given by the C4-C1–Cβ-Cα dihedral angle with pivot point at the forming C1-Cβ bond; positive angles represent inward twist by the dienophile, negative angle is outward twist.

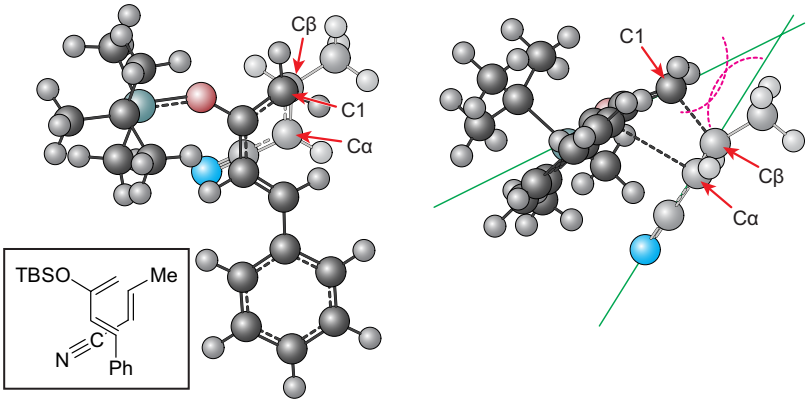

Figure 3. *Endo* transition state structures for cycloaddition of 8 and 18 optimized by B3LYP showing the diene–dienophile overlay (left) and the tilt of the dienophile with respect to the plane of the diene (right, approximated by green lines). The inset structure is included for clarity. Diene **8** is shown in a darker shade than the dienophiles **18**.

such repulsive forces, likely more readily for the *exo* pathway. The effect of the strong steric repulsion found in the *endo* transition states may be two-fold. On one hand, it raises the $\Delta E_d^{\ddagger}$ of the *endo* pathway to the extent that possible stabilization from secondary orbital interactions might be overwhelmed. On the other hand, the secondary orbital interaction itself may be reduced when close alignment is not geometrically favored. In addition, the *endo* transition state may also involve extra electrostatic repulsion between the electron-withdrawing group of the dienophiles and the silyloxy group of the dienes[10,25]. This repulsion is amplified by the presence of appropriately positioned electron-rich atoms in the electron-withdrawing group, such as in the nitrile, ester, and even nitro functionalities. Given the experimentally and computationally observed *exo* selectivity trend relating to the electron-withdrawing group, the degree of destabilization of the *endo* transition states can be proportionately explained by the combination of the size and electronegativity of such electron-withdrawing group.

Conclusions

We have noted and systematically investigated a number of *exo*-selective thermal normal-electron-demand Diels–Alder reactions involving 2-silyloxydienes substituted at the terminal positions and simple dienophiles with a range of substitution patterns. These variations in the reacting partners fleshed out the salient factors that permitted such unconventional *exo* selectivity. Structural features such as substitution at Cβ, but not at the

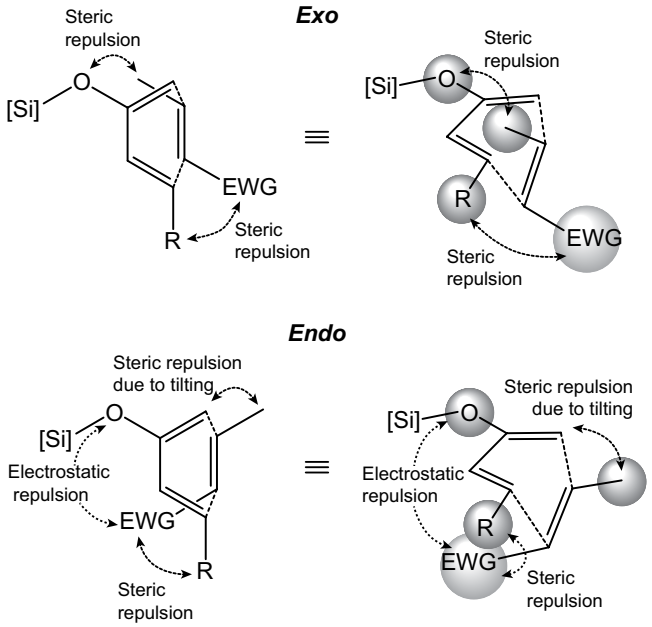

Figure 4. Proposed major rivalling interaction forces in the two pathways of the examined normal-electron demand Diels–Alder reactions.

Cα position of the dienophile and the presence of nitrile and ester electron-withdrawing groups favour the *exo* adduct. Such observations are the likely result of the stress on the Cβ-substituent and the electrostatic and steric repulsions experienced by the corresponding electron-withdrawing group in the *endo* transition state. The larger distortion experienced in the *endo* pathway as a consequence of repulsive forces is consistent with the diminished preference for the *endo* product, even overriding the stabilizing interaction forces in many of the studied cases. Overall, the present work brings important insights into the intricate *exo*/*endo* selectivity mechanics of the Diels–Alder cycloadditions. The findings in this report may help guide chemists in their pursuit of wielding this celebrated and very useful reaction.

Methods

Chemical synthesis. The complete experimental details and compound characterization can be found in the Supplementary Methods. For the NMR spectra of the compounds in this article, see Supplementary Figs 7–270.

Computation. Density functional theory calculations were carried out with *Gaussian09*[49] using the B3LYP and M06-2X hybrid functionals with the 6-311++G(d,p) basis set. Transition state optimizations were performed using the Synchronous Transit-Guided Quasi-Newton (STQN) method[50,51]. Harmonic vibrational frequencies were computed for all optimized structures to ensure that they are either potential energy surface minima (all real frequencies) or transition states (one imaginary frequency). Zero-point energies were included in all thermodynamic quantities at 298 K. Product distributions at room temperature were calculated using the Arrhenius rate expression derived from the standard transition state theory[52]. Solvation corrections for the solvent used in most experiments (xylene, *o*-, *m*-, *p*-mixture, $\varepsilon = 2.3879$) were calculated using the polarizable continuum model (PCM) method[53] with default universal force field (UFF) radii.

Data availability. The X-ray crystallographic coordinates for compounds **exo-10**, **exo-11**, **exo-31**, **endo-62**, **exo-64** and **exo-67** in this study have been deposited at the Cambridge Crystallographic Data Centre (CCDC), under deposition numbers CCDC 1450387, CCDC 1450388, CCDC 1450389, CCDC 1450392, CCDC 1450390 and CCDC 1450391, respectively. This data can be obtained free of charge from the CCDC via www.ccdc.cam.ac.uk/data_request/cif.

References

1. Diels, O. & Alder, K. Synthesen in der hydroaromatischen reihe. *Justus Liebigs Ann. Chem.* **460,** 98–122 (1928).
2. Fringuelli, F. & Taticchi, A. *The Diels–Alder Reaction: Selected Practical Methods* (Wiley, Chichester, UK, 2002).
3. Nicolaou, K. C., Snyder, S. A., Montagnon, T. & Vassilikogiannakis, G. The Diels–Alder reaction in total synthesis. *Angew. Chem. Int. Ed.* **41,** 1668–1698 (2002).
4. Takao, K., Munakata, R. & Tadano, K. Recent advances in natural product synthesis by using intramolecular Diels–Alder reactions. *Chem. Rev.* **105,** 4779–4807 (2005).
5. Funel, J.-A. & Abele, S. Industrial applications of the Diels–Alder reaction. *Angew. Chem. Int. Ed.* **52,** 3822–3863 (2013).
6. Nawrat, C. C. & Moody, C. J. Quinones as dienophiles in the Diels–Alder reaction: history and applications in total synthesis. *Angew. Chem. Int. Ed.* **53,** 2056–2077 (2014).
7. Hoffmann, R. & Woodward, R. B. Orbital symmetries and *endo-exo* relationships in concerted cycloaddition reactions. *J. Am. Chem. Soc.* **87,** 4388–4389 (1965).

8. Wannere, C. S. *et al.* The existence of secondary orbital interactions. *J. Comput. Chem.* **28,** 344–361 (2007).
9. Roush, W. R. & Brown, B. B. Enantioselective synthesis of 2-alkyl-5-methylene-1,3-dioxolan-4-ones and *exo*-selective Diels-Alder reactions with cyclopentadiene. *J. Org. Chem.* **57,** 3380–3387 (1992).
10. Node, M. *et al. Exo* selective Diels–Alder reaction of nitroolefins with Danishefsky's diene. *Chem. Commun.* 2559–2560 (1996).
11. Kozmin, S. A. & Rawal, V. H. Preparation and Diels–Alder reactivity of 1-amino-3-siloxy-1,3-butadienes. *J. Org. Chem.* **62,** 5252–5253 (1997).
12. Jung, M. E. & Nishimura, N. Stereoselective formation of formal *exo* Diels–Alder adducts of silyloxydienes and allenecarboxylates. *J. Am. Chem. Soc.* **121,** 3529–3530 (1999).
13. Fotiadu, F., Pardigon, O., Buono, G., Le Corre, M. & Hercouët, A. Efficient synthesis of 3-methylene-2-pyrrolidinone and highly exoselective Diels-Alder addition to cyclopentadiene. *Tetrahedron Lett.* **40,** 867–870 (1999).
14. Boren, B. *et al. Exo*-selective Diels–Alder reactions of vinylazepines. Origin of divergent stereoselectivity in Diels–Alder reactions of vinylazepines, vinylpiperideines, and vinylcycloalkenes. *J. Org. Chem.* **68,** 8991–8995 (2003).
15. Cernak, T. A. & Gleason, J. L. Density functional theory guided design of *exo*-selective dehydroalanine dienophiles for application toward the synthesis of palau'amine. *J. Org. Chem.* **73,** 102–110 (2008).
16. Corey, E. J. & Loh, T. P. First application of attractive intramolecular interactions to the design of chiral catalysts for highly enantioselective Diels–Alder reactions. *J. Am. Chem. Soc.* **113,** 8966–8967 (1991).
17. Yoon, T., Danishefsky, S. J. & de Gala, S. A concise total synthesis of (±)-mamanuthaquinone by using an *exo*-Diels–Alder reaction. *Angew. Chem. Int. Ed. Engl.* **33,** 853–855 (1994).
18. Maruoka, K., Imoto, H. & Yamamoto, H. *Exo*-selective Diels–Alder reaction based on a molecular recognition approach. *J. Am. Chem. Soc.* **116,** 12115–12116 (1994).
19. Powers, T. S. *et al.* Asymmetric *exo*-selective Diels–Alder reactions by steric attenuation of secondary orbital interactions. *J. Am. Chem. Soc.* **119,** 6438–6439 (1997).
20. Kawamura, M. & Kudo, K. *Exo*-selective asymmetric Diels–Alder reaction of acrylate ester. *Chirality* **14,** 727–730 (2002).
21. Cannizzaro, C. E., Ashley, J. A., Janda, K. D. & Houk, K. N. Experimental determination of the absolute enantioselectivity of an antibody-catalyzed Diels–Alder reaction and theoretical explorations of the origins of stereoselectivity. *J. Am. Chem. Soc.* **125,** 2489–2506 (2003).
22. Sammis, G. M., Flamme, E. M., Xie, H., Ho, D. M. & Sorensen, E. J. Design, synthesis, and reactivity of 1-hydrazinodienes for use in organic synthesis. *J. Am. Chem. Soc.* **127,** 8612–8613 (2005).
23. Qi, J. & Roush, W. R. Synthesis of precursors of the agalacto (*exo*) fragment of the quartromicins via an auxiliary-controlled *exo*-selective Diels–Alder reaction. *Org. Lett.* **8,** 2795–2798 (2006).
24. Sudo, Y., Shirasaki, D., Harada, S. & Nishida, A. Highly enantioselective Diels–Alder reactions of Danishefsky type dienes with electron-deficient alkenes catalyzed by Yb(III)-BINAMIDE complexes. *J. Am. Chem. Soc.* **130,** 12588–12589 (2008).
25. Lam, Y.-H. *et al.* Diels–Alder *exo* selectivity in terminal-substituted dienes and dienophiles: experimental discoveries and computational explanations. *J. Am. Chem. Soc.* **131,** 1947–1957 (2009).
26. Liu, Z. *et al.* Unique steric effect of geminal bis(silane) to control the high *exo*-selectivity in intermolecular Diels–Alder reaction. *J. Am. Chem. Soc.* **138,** 1877–1883 (2016).
27. Ahrendt, K. A., Borths, C. J. & MacMillan, D. W. C. New strategies for organic catalysis: the first highly enantioselective organocatalytic Diels–Alder reaction. *J. Am. Chem. Soc.* **122,** 4243–4244 (2000).
28. Ishihara, K. & Nakano, K. Design of an organocatalyst for the enantioselective Diels–Alder reaction with α-acyloxyacroleins. *J. Am. Chem. Soc.* **127,** 10504–10505 (2005).
29. Kano, T., Tanaka, Y. & Maruoka, K. *Exo*-selective asymmetric Diels–Alder reaction catalyzed by diamine salts as organocatalysts. *Chem. Asian J.* **2,** 1161–1165 (2007).
30. Gotoh, H. & Hayashi, Y. Diarylprolinol silyl ether as catalyst of an *exo*-selective, enantioselective Diels–Alder reaction. *Org. Lett.* **9,** 2859–2862 (2007).
31. Li, J.-L., Liu, T.-Y. & Chen, Y.-C. Aminocatalytic asymmetric Diels–Alder reactions via HOMO activation. *Acc. Chem. Res.* **45,** 1491–1500 (2012).
32. Dossetter, A. G., Jamison, T. F. & Jacobsen, E. N. Highly enantio- and diastereoselective hetero-Diels-Alder reactions catalyzed by new chiral tridentate chromium(III) catalysts. *Angew. Chem. Int. Ed.* **38,** 2398–2400 (1999).
33. Lestini, E., Robertson, K., Murphy, C. D. & Paradisi, F. Alternative mild route to the synthesis of 4-methylenecyclohex-2-enone, a key moiety of the anticancer compounds ottelione A and B. *Synth. Commun.* **42,** 1864–1876 (2012).
34. Lee, M. W. & Herndon, W. C. Stereochemistry of the furan-maleic anhydride cycloaddition. *J. Org. Chem.* **43,** 518 (1978).
35. Nakashima, D. & Yamamoto, H. Design of chiral N-triflyl phosphoramide as a strong chiral Brønsted acid and its application to asymmetric Diels–Alder reaction. *J. Am. Chem. Soc.* **128,** 9626–9627 (2006).
36. Becke, A. D. J. Density-functional thermochemistry. III. The role of exact exchange *Chem. Phys.* **98,** 5648–5652 (1993).
37. Lee, C., Yang, W. & Parr, R. G. Development of the Colle-Salvetti correlation-energy formula into a functional of the electron density. *Phys. Rev. B* **37,** 785–789 (1988).
38. Zhao, Y. & Truhlar, D. The M06 suite of density functionals for main group thermochemistry, thermochemical kinetics, noncovalent interactions, excited states, and transition elements: two new functionals and systematic testing of four M06-class functionals and 12 other functionals. *Theor. Chem. Acc.* **120,** 215–241 (2008).
39. Hehre, W. J., Ditchfield, R. & Pople, J. A. Self-consistent molecular orbital methods. XII. Further extensions of Gaussian-type basis sets for use in molecular orbital studies of organic molecules. *J. Chem. Phys.* **56,** 2257 (1972).
40. Hariharan, P. C. & Pople, J. A. The influence of polarization functions on molecular orbital hydrogenation energies. *Theor. Chim. Acta* **28,** 213 (1973).
41. Pieniazek, S. N., Clemente, F. R. & Houk, K. N. Sources of error in DFT computations of C–C bond formation thermochemistries: $\pi \rightarrow \sigma$ transformations and error cancellation by DFT methods. *Angew. Chem. Int. Ed.* **47,** 7746–7749 (2008).
42. Guner, V. *et al.* A standard set of pericyclic reactions of hydrocarbons for the benchmarking of computational methods: the performance of ab initio, density functional, CASSCF, CASPT2, and CBS-QB3 methods for the prediction of activation barriers, reaction energetics, and transition state geometries. *J. Phys. Chem. A* **107,** 11445–11459 (2003).
43. Ajaz, A. *et al.* Concerted vs stepwise mechanisms in dehydro-Diels–Alder reactions. *J. Org. Chem.* **76,** 9320–9328 (2011).
44. Ess, D. H. & Houk, K. N. Distortion/interaction energy control of 1,3-dipolar cycloaddition reactivity. *J. Am. Chem. Soc.* **129,** 10646–10647 (2007).
45. Fernández, I. Combined activation strain model and energy decomposition analysis methods: a new way to understand pericyclic reactions. *Phys. Chem. Chem. Phys.* **16,** 7662–7671 (2014).
46. Arrieta, A., Cossío, F. P. & Lecea, B. Direct evaluation of secondary orbital interactions in the Diels–Alder reaction between cyclopentadiene and maleic anhydride. *J. Org. Chem.* **66,** 6178–6180 (2001).
47. Singleton, D. A. *et al.* Isotope effects and the distinction between synchronous, asynchronous, and stepwise Diels–Alder reactions. *Tetrahedron* **57,** 5149–5160 (2001).
48. Brown, F. K. & Houk, K. N. The influence of substituent induced asynchronicity on the stereochemistries of intramolecular Diels–Alder reactions. *Tetrahedron Lett.* **26,** 2297–2300 (1985).
49. Frisch, M. J. *et al. Gaussian 09, revision C.01* (Gaussian Inc, Wallingford, CT, 2009).

50. Peng, C. & Schlegel, H. B. Combining synchronous transit and quasi-Newton methods to find transition states. *Israel J. Chem.* **33,** 449–454 (1993).
51. Peng, C., Ayala, P. Y., Schlegel, H. B. & Frisch, M. H. Using redundant internal coordinates to optimize equilibrium geometries and transition states. *J. Comput. Chem.* **17,** 49–56 (1996).
52. Moore, J. W. & Pearson, R. G. *Kinetics and Mechanism* 3rd ed. Ch. 7 (Wiley, New York, 1981).
53. Tomasi, J. & Persico, M. Molecular interactions in solution: an overview of methods based on continuous distributions of the solvent. *Chem. Rev.* **94,** 2027–2094 (1994)

Acknowledgements

This work was supported by the Ministry of Science and Technology (MOST 103-2113-M-003-006-MY2, MOST 104-2628-M-001-001, MOST 104-0210-01-09-02, MOST 105-0210-01-13-01 and MOST 105-2113-M-003-008) and Academia Sinica. C.-J.H. and E.Y.-T.L. thank National Center for High-performance Computing (NCHC) of Taiwan for the help on computational resources.

Author Contributions

S.-C.H. designed the synthetic experiments and supervised students and staffs. G.-M.H., S.-K.H., T.W. and K.B.W. performed the synthetic experiments. C.-J.H. carried out the computational work under the supervision of E.Y.-T.L. M.M.L.Z. assisted in the data interpretations and wrote the manuscript. All authors reviewed the manuscript.

Additional Information

Supplementary information accompanies this paper at http://www.nature.com/srep

Competing financial interests: The authors declare no competing financial interests.

How to cite this article: Ho, G.-M. *et al.* Unconventional *exo* selectivity in thermal normal-electron-demand Diels–Alder reactions. *Sci. Rep.* **6**, 35147; doi: 10.1038/srep35147 (2016).